

J1.6 OBSERVATIONS OF STRATIFIED ATMOSPHERIC SHEAR-DRIVEN TURBULENCE AT LOW AND HIGH RICHARDSON NUMBERS

Thorsten Mauritsen and Gunilla Svensson
 Department of Meteorology at Stockholm University, Sweden

Near the Earth's surface, in the planetary boundary layer, turbulence is the main factor controlling the vertical exchange of momentum, heat trace substance. Stably stratified boundary layers (SBL) occur, for instance, over land during night-time or when warm air is advected over a cold surface. Strong stable stratification serves to suppress turbulent motions, hereby reducing the magnitude of the turbulent fluxes. This lowers the SBL height, which may be as shallow as a few meters (e.g. Mahrt, 1999; Poulos et al. 2002).

Observational studies of the SBL have used different stability parameters to characterize the extent to which the flow is dominated by stratification. For instance the widely used Monin-Obukhov stability parameter, z/L , is calculated from the turbulent fluxes of momentum and heat (Obukhov, 1946). Studies based upon this stability parameter (e.g. Businger et al. 1971; Nieuwstadt 1984; Mahrt et al. 1998; Pahlow et al. 2001; Klipp and Mahrt, 2004 and Grachev et al. 2005) have made significant contributions to our knowledge of the SBL (Sorbjan, 2006). These studies result in empirical relationships between the mean profiles of wind and temperature and the turbulent fluxes (e.g. Louis, 1979; Delage, 1997). However, the interpretation of these studies is complicated by the fact that the method suffers from self-correlations (e.g. Hicks, 1978; Mahrt et al. 1998; Andreas and Hicks, 2002; Klipp and Mahrt, 2004 and Baas et al. 2006).

An alternative to using z/L is to evaluate the gradient of the mean potential density and the mean wind (Richardson, 1920). This was proposed for instance by Klipp and Mahrt (2004). The gradient Richardson number is defined:

$$Ri = \frac{N^2}{S^2},$$

where N is the Brunt-Väisälä frequency and S is the vertical wind-shear. This method does not suffer from self-correlation, and allows the study of the properties of turbulence even at

strong flow stability.

DATASETS

We used data from CASES-99 (Poulos et al. 2002), SHEBA (Uttal et al. 2002), CME, FLOSS, FLOSSII (Mahrt and Vickers, 2005) and a Swedish experiment performed on the coast of the island Östergarnsholm (OGH) in the Baltic sea (Smedman et al. 2003), see Figure 1. Thus, we sample a vast variety of physical environments: Grassland, Arctic sea ice, mountain forest canopy, partially snow covered land and coastal conditions. The total amount is the equivalent of five and a half years worth of stably stratified turbulence data.

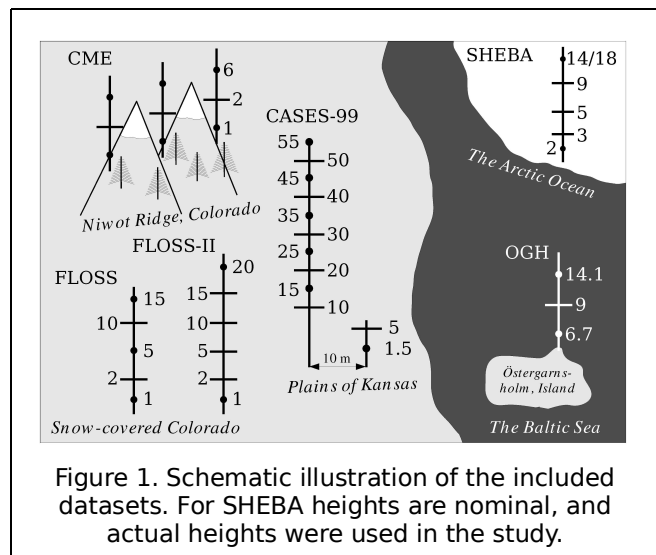


Figure 1. Schematic illustration of the included datasets. For SHEBA heights are nominal, and actual heights were used in the study.

For each sonic anemometer Ri is estimated using measurements immediately above and below the level of interest. In Figure 1 the lines are the sonic levels, usually including temperature measurements, while dots are levels with slow-response instrumentation only. Turbulent second moments were calculated by the researchers that provided the data, including their quality checks and plane-rotations. In CASES-99, CME, FLOSS and FLOSSII 5-minute means were used, while SHEBA used 10-minute means, averaged over 1 hour and OGH used 10-minute running means, also over 1 hour.

In the current study entities are non-dimensionalized before averaging. For example, in Figure 2, the stress, τ , is normalized by the turbulent kinetic energy (E). Mauritsen and Svensson (2006) explored the possibility of using vertical variance, but the results were insignificantly different from the subset of plots presented here. See Mauritsen and Svensson (2006) for more detailed information.

RESULTS

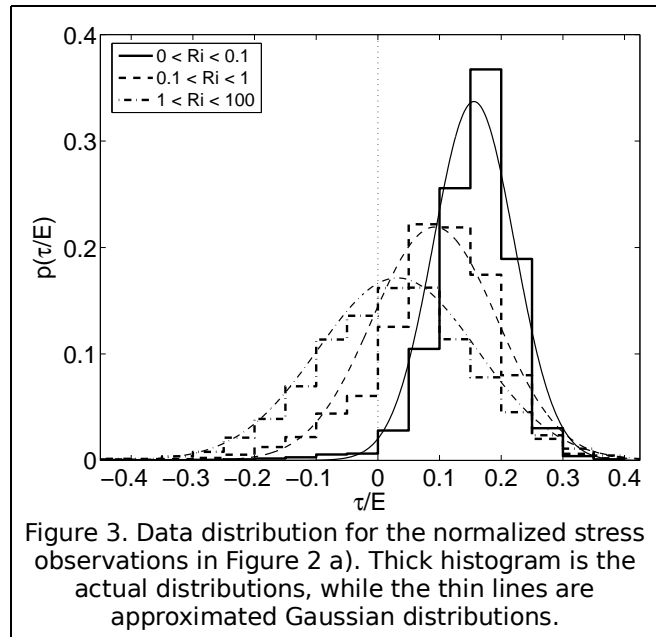
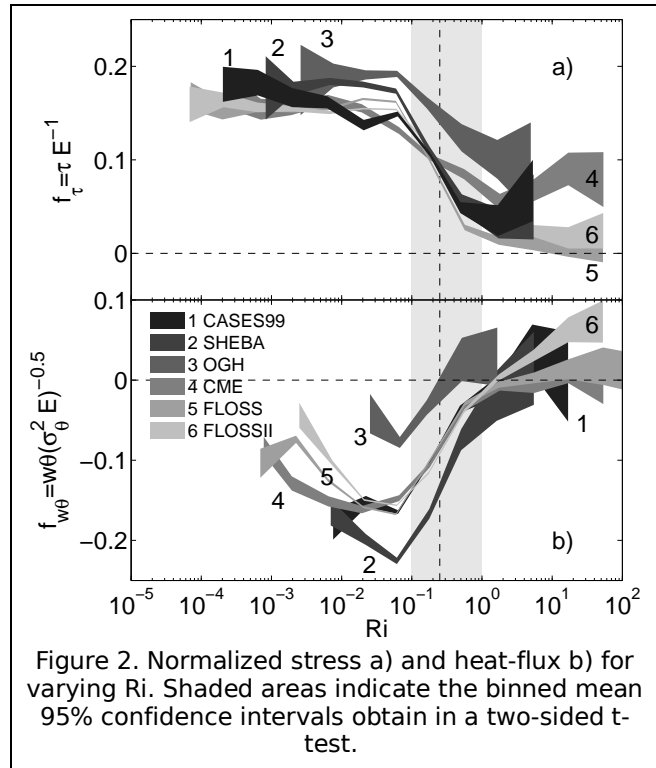
Figure 2 shows the normalized stress and heat flux variation with Ri. We find that at $Ri < 0.1$, the stress is almost proportional to the turbulent kinetic energy. At $0.1 < Ri < 1$ the proportionality decreases rapidly to a new lower level. While all mean stresses are positive at $Ri > 1$, one of the six datasets has a 95% confidence interval that includes zero. However, we can say with high confidence that there is a non-zero stress at large Ri, rejecting the hypothesis of non-turbulence (e.g. Richardson, 1920; Miles, 1961; Howard, 1961, Chandrasekhar, 1961) for atmospheric data.

The scatter among the datasets for the normalized turbulent heat-flux is larger, and hence more difficult to interpret. The main reason for this is low signal-to-noise ratios at small Ri. However, there is indication of a transition from a finite level at $Ri < 0.1$ to another level at $Ri > 1$. At large Ri all but one dataset has 95% confidence intervals including zero. The FLOSSII dataset exhibits up-gradient heat-fluxes at large Ri.

One possible explanation for this behaviour is that during that particular experiment, sage brush was present upstream from the tower, which was surrounded by snow-covered grass, causing the flow to be horizontally inhomogeneous (Mahrt and Vickers, 2005).

An important point in the present study is that we keep observations which indicate up-gradient fluxes of both heat and momentum. While these observations do not obey Monin-Obukhov similarity theory, they are part of the ensemble-distribution. Figure 3 shows the normalized stress for three different intervals. The observed distributions are close to Gaussian, justifying the application of the two-sided t-test and the validity of the mean value. For near-neutral conditions the distribution

hardly includes any negative stress observations, while at large Ri close to half the observed values are negative. Removing these values would lead to highly biased mean values. In Monin-Obukhov based studies these observations are usually *a priori* rejected.



The results for the heat-flux are further

supported by the water vapour flux, displayed in Figure 4. Here we analyzed data from the 5-meter level in CASES-99. During this particular campaign the water vapour mixing ratio was always larger close to the ground than at higher levels, causing the flux to be on average upward. For the water vapour flux we don't have the same signal-to-noise problem as for the heat-flux in near-neutral conditions. Here a clear proportionality between flux and variance is evident at $Ri < 0.1$. At large Ri the water vapour flux cannot be distinguished from zero.

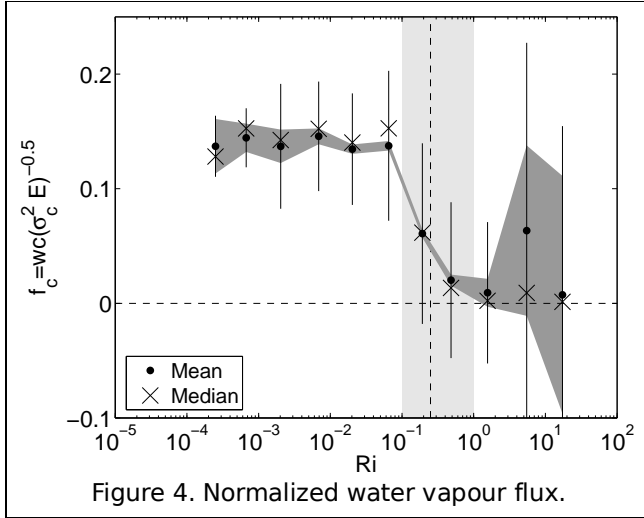


Figure 4. Normalized water vapour flux.

The observed atmospheric turbulence is not isotropic as can be seen in Figure 5. Here we plotted the ratio of horizontal to vertical variance. At $Ri < 0.1$ the ratios range from 5-8 while isotropic turbulence has a value of 2. At $Ri > 1$ this value increases considerably. Four of the datasets have values of 12-15, while the two extreme datasets are OGH and FLOSS.

Finally, we inspect the ratio of turbulent potential energy to vertical variance in figure 6. The turbulent potential energy is defined:

$$P = \frac{g}{\theta^2} \frac{\sigma_\theta^2}{2N^2},$$

where g is gravity and θ is the mean potential temperature. Unfortunately, both P and Ri contain N . Thus, plots of this P vs. Ri would be subject to self-correlation, unless special care is taken. To avoid this problem we use different measurements of N on each axis. For the CASES-99 dataset this is possible for levels 20, 30 and 40 meters above ground. Referring to

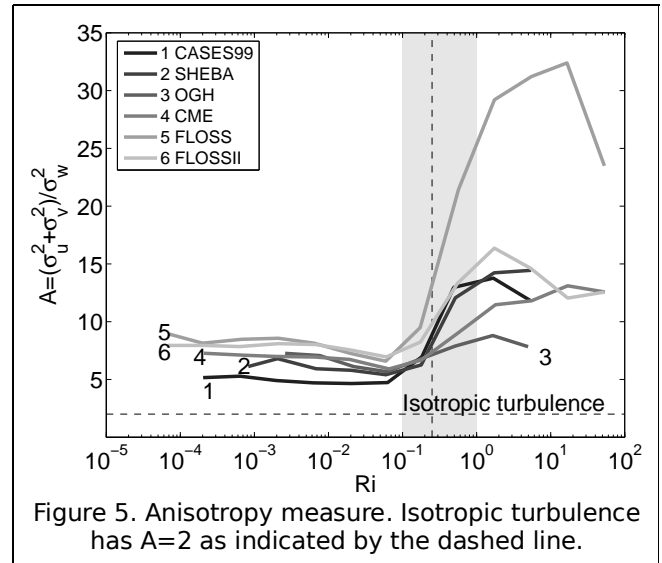


Figure 5. Anisotropy measure. Isotropic turbulence has $A=2$ as indicated by the dashed line.

Figure 1, for the 20-meter level we used temperatures from 15 and 25 (Inner), and 10 and 30-meter levels (Outer), respectively, to obtain two statistically independent estimates of N . For example for the solid curve we used the 'Outer' estimates of N for Ri , while we used the 'Inner' gradients for P .

In Figure 6 we plotted both the self-correlated curve, along with Ri from the inner- and P from the outer gradient and vice versa. It is clear that self-correlation causes an unrealistic behaviour at small Ri . This can be easily understood. Since N appears in the denominator of P , a small N caused by a random error will result in a large P -value. The other two curves in Figure 6 are with independent estimates of N . Both tend to zero at small Ri .

At increasing Ri , all three curves exhibit a transition to a new level of about 3-4 at $Ri > 1$. The transition appears at slightly different Ri , since the inner temperature gradient can be larger than the outer gradient. This is somewhat larger than the value of 2.5 found by Schumann and Gerz (1995). Combining this level with Figure 5 we get P/E about 0.5, which is lower than the theoretical prediction of unity, for a pure gravity wave field in the absence of rotation (Nappo, 2002).

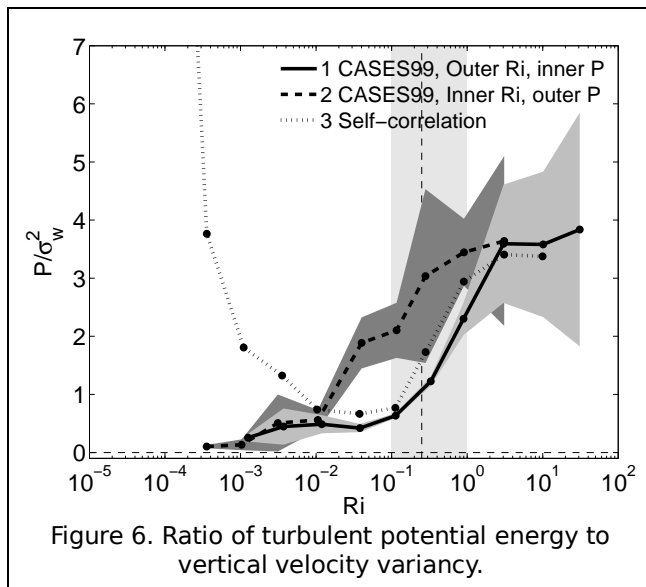


Figure 6. Ratio of turbulent potential energy to vertical velocity variance.

CONCLUSIONS

We have analyzed a collection of six datasets with a total worth of 5.5 years of observed stably stratified turbulence. The data were collected in physically very different conditions, with various instrumentation and mast-setup and they were prepared by different researchers, applying different post-processing algorithms. All of which may contribute to differences among the datasets. Several common features are identified despite these complicating factors.

We find that two important regimes exist, the *weakly-* and *very stratified* regimes, in accordance with Mahrt et al. (1998). We find that at $Ri < 0.1$, non-dimensional fluxes are almost constant. At $0.1 < Ri < 1$ a transition occurs where scaled fluxes decrease rapidly. For very stratified conditions, $Ri > 1$, the momentum flux is still finite, while fluxes of heat and moisture cannot be distinguished from zero using the present approach. At the same time horizontal velocity modes increasingly dominates over vertical velocity, and turbulent potential energy increases to about half of the turbulent kinetic energy at $Ri > 1$.

One may speculate that the transition to the very stable regime is Nature's way of upholding turbulence, even at strong flow stability.

REFERENCES

• Andreas, E. L., B. B. Hicks, 2002. Comments

on "Critical Test of the validity of Monin Obukhov Similarity during Convective Conditions". *J. Atmos. Sci.* **59**, 2605-2607.

- Baas, P., G.J. Steeneveld, B.J.H. van de Wiel, and A.A.M. Holtslag, 2006: Exploring Self-correlation in flux-gradient relationships for stably stratified conditions, *J. Atmos. Sci.*, in press.
- Businger, J. A. et al. 1971. Flux-profile relationships in the atmospheric surface layer. *J. Atmos. Sci.* **28**, 181-189.
- Chandrasekhar, S. 1961. Hydrodynamic and hydromagnetic stability, 103. *Oxford University Press*.
- Cuxart, J. et al. 2006. Single-column model intercomparison for a stably stratified boundary layer. *Bound-Layer Meteorol.* in press.
- Delage, Y. 1997. Parameterising sub-grid scale vertical transport in atmospheric models under stable stratification. *Bound-Layer Meteorol.* **82**, 23-48.
- Grachev, A. A. et al. 2005. Stable boundary-layer scaling regimes: The SHEBA data. *Bound-Layer Meteorol.* **116**, 201-235.
- Hicks, B. B. 1978. Some limitations of dimensional analysis and power laws. *Bound-Layer Meteorol.* **14**, 567-569.
- Howard, L. N. 1961. Note on paper by John W. Miles. *J. Fluid Mech.* **10**, 509-512.
- Klipp, C. L. and L. Mahrt, 2004. Flux-gradient relationships, self-correlation and intermittency in the stable boundary layer. *Quart. J. Roy. Meteor. Soc.* **130**, 2087-2103.
- Louis, J. F. 1979. A parametric model of vertical eddy fluxes in the atmosphere. *Bound-Layer Meteorol.* **17**, 187-202.
- Mahrt, L. 1999. Stratified atmospheric boundary layers. *Bound-Layer Meteorol.* **90**, 375-396.
- Mahrt et al. 1998. Nocturnal boundary layer regimes. *Bound-Layer Meteorol.* **88**, 255-278.
- Mahrt, L. and D. Vickers 2005. Boundary layer adjustment over small-scale changes in surface heat-flux. *Bound-Layer Meteorol.* **116**, 313-330.
- Mauritsen, T. and G. Svensson, 2006. Observations of stably stratified shear-driven atmospheric turbulence at low and high Richardson numbers. *Manuscript*.
- Miles, J. 1961. On the stability of heterogeneous shear flows. *J. Fluid Mech.* **10**, 496-508.

- Nappo, C. J. 2002. An introduction to atmospheric gravity waves. *Academic Press*, pp. 260.
- Nieuwstadt, F. T. M. 1984. The turbulent structure of the stable, nocturnal boundary layer. *J. Atmos Sci.*, **41**, 2202-2216.
- Obukhov, A. M. 1946. Turbulence in an atmosphere with inhomogeneous temperature. *Tr. Inst. Teor. Geofiz. Akad. Nauk SSSR*, **1**, 95-115.
- Pahlow, M. et al. 2001. On Monin-Obukhov similarity in the stable atmospheric boundary layer. *Bound-Layer Meteorol.* **99**, 225-248.
- Poulos, G. S. et al. 2002. CASES-99: A comprehensive investigation of the stable nocturnal boundary layer. *Bull. Amer. Meteor. Soc.* **83**, 555-581.
- Richardson, L. F. 1920. The supply of energy from and to atmospheric eddies. *Proc. R. Soc.* **A97**, 354-373.
- Schumann, U. and T. Gerz, 1995. Turbulent mixing in stably stratified shear flows. *J. Appl. Meteorol.* **34**, 33-48.
- Smedman et al. 2003. Effect of sea state on the momentum exchange over the sea during neutral conditions. *J. Geophys. Res.* **108**(C11), 3367.
- Sorbjan, Z. 2006. Local structure of turbulence in stably-stratified boundary layers. *J. Atmos Sci.*, in press.
- Uttal, T. et al. 2002. Surface heat budget of the Arctic Ocean. *Bull. Amer. Meteor. Soc.* **83**, 255-275.